Biochimica et Biophysica Acta 1838 (2014) 2503–2510

Contents lists available at ScienceDirect

Biochimica et Biophysica Acta

journal homepage: www.elsevier.com/locate/bbamem

Fluid domain patterns in free-standing membranes captured on a solid support

Tripta Bhatia [a,b], Peter Husen [a,1], John H. Ipsen [a,b], Luis A. Bagatolli [a,c], Adam Cohen Simonsen [a,b,*]

[a] MEMPHYS — Center for Biomembrane Physics, University of Southern Denmark (SDU), 5230 Odense M, Denmark
[b] Department of Physics Chemistry and Pharmacy, SDU
[c] Department of Biochemistry and Molecular Biology, SDU

ARTICLE INFO

Article history:
Received 16 December 2013
Received in revised form 3 May 2014
Accepted 16 May 2014
Available online 24 May 2014

Keywords:
Membranes
Rafts
Giant unilamellar vesicles
Domains
AFM

ABSTRACT

We devise a methodology to fixate and image dynamic fluid domain patterns of giant unilamellar vesicles (GUVs) at sub-optical length scales. Individual GUVs are rapidly transferred to a solid support forming planar bilayer patches. These are taken to represent a fixated state of the free standing membrane, where lateral domain structures are kinetically trapped. High-resolution images of domain patterns in the liquid-ordered (l_o) and liquid-disordered (l_d) co-existence region in the phase-diagram of ternary lipid mixtures are revealed by atomic force microscopy (AFM) scans of the patches. Macroscopic phase separation as known from fluorescence images is found, but with superimposed fluctuations in the form of nanoscale domains of the l_o and l_d phases. The size of the fluctuating domains increases as the composition approaches the critical point, but with the enhanced spatial resolution, such fluctuations are detected even deep in the coexistence region. Agreement between the area-fraction of domains in GUVs and the patches respectively, supports the assumption that the thermodynamic state of the membrane remains stable. The approach is not limited to specific lipid compositions, but could potentially help uncover lateral structures in highly complex membranes.

1. Introduction

The conundrum of cholesterol-rich membrane-domains as carriers of biological activity is facing a number of challenges related to the length and time-scale of such domains. The initially proposed *raft*-hypothesis [1] based on static sphingolipid–cholesterol domains as platforms for GPI-anchored proteins found a justification in membrane biophysics as a realization of thermodynamic phase separation between l_o and l_d phases of cholesterol-containing bilayers and monolayers [2,3]. However, while large macroscopic domains are not observed in the plasma membrane, the evidence for a crucial role of cholesterol and sphingolipids in multiple membrane functions is mounting [4,5]. If such lipid-mediated effects are associated with membrane domains, their size must be small, well below the optical diffraction limit of ~200 nm. Here spectroscopic techniques like NMR and ESR [6] provide the main source of information and thus indirect evidence about the lateral membrane structure. Recent experimental studies of *rafts*, using stimulated emission depletion (STED) far-field fluorescence microscopy, claim presence of 20 nm domains in the plasma membrane where proteins reside for 10–20 ms [7]. Such small-scale structures are local and short lived, which impose a challenge for their experimental observation, and only few tools for their imaging are available. For example, AFM and STED microscopy are promising techniques for imaging of nanoscale membrane structures. These high-resolution imaging methods require membrane fixation either by a solid support or by a chemical cross-linking. However, it is well known that solid-supported membranes are subject to perturbations from the substrate. Concrete manifestations of such effects may be a reduction in the lipid diffusion coefficient [8], an increased phase transition temperature [9], different domain-size distributions and slower coarsening dynamics in membranes with phase separation [10]. This may also influence the organization of membrane curvature active components [11] and protein organization mediated by membrane conformational fluctuations [12]. Therefore, results on membrane domains obtained on a supported membrane cannot implicitly be assumed to represent the equivalent free standing membrane [3, 13–15]. In fact, the very purpose of membrane fixation is to decrease membrane fluctuations, both in-plane and out-of-plane. The dilemma has been that available high-resolution imaging techniques are often only applicable to supported membranes while information on the free-standing analog is wanted. In this work we aim to resolve this dilemma by avoiding the solid substrate during sample preparation and instead explore the support as a tool to rapidly immobilize domain features in free-standing membranes

* Corresponding author at: MEMPHYS — Center for Biomembrane Physics, University of Southern Denmark, 5230 Odense M, Denmark.
E-mail address: adam@memphys.sdu.dk (A.C. Simonsen).
[1] Now at: EmaZys Technologies ApS, Vejle, Denmark.

http://dx.doi.org/10.1016/j.bbamem.2014.05.016
0005-2736/

of equilibrated GUVs. With this approach we characterize fluid domain patterns in collapsed GUVs using high resolution imaging with AFM.

An additional challenge for membrane biophysics is to establish a framework for explaining the prevalence of small-scale membrane domains. It has been proposed that l_o, l_d critical point fluctuations may provide such a framework [16]. But true critical fluctuations require finely tuned thermodynamic conditions, which are delicate to maintain in a biomembrane. The results presented here point to the existence of a previously undetected population of microscale and nanoscale domains in ternary membranes. If such small domains are also present in a free-standing membrane they may represent thermal fluctuations characterized by formation of small minority phase domains deep inside the coexistence region and far from the critical point. The observations are similar to the findings for the related *main* transition of one and two-component PC-lipid bilayer systems [17–19], where lateral density and compositional fluctuations give rise to dynamic membrane heterogeneity in a wide range of system conditions around the phase transition/coexistence. The presence of a nearby l_o,l_d co-existence is a much less restrictive thermodynamic condition to fulfill than proximity to a critical point.

2. Materials and methods

1,2-Dioleoyl-sn-glycero-3-phosphocholine (DOPC), cholesterol and 1,2-dipalmitoyl-sn-glycero-3-phosphocholine (DPPC) were purchased from Corden-Pharma. The fluorescence probes, N-Lissamine rhodamine B 1,2-dihexadecanoyl-sn-glycero-3-phosphoethanolamine, triethylammonium salt (RhPE) and Napthopyrene (NaP) were purchased from Molecular Probes and Sigma respectively. Chloroform was of HPLC grade quality purchased from Rathburn (Micro-lab, Aarhus, Denmark). 1 mM stock solutions in chloroform of each lipid and each dye are prepared separately. Phosphorous analysis of the lipid samples was performed. Ternary mixtures with molar ratio of DOPC:DPPC:cholesterol (3:5:2), (3.5:3.5:3) and (4:2:4), corresponding to the compositions *I*, *II*, and *III* respectively, were prepared using the 1 mM stock solutions. The dye solutions were added to the ternary mixtures such that the dye/lipid molar fraction is 0.8%. We have tested for the possible influence of the probe on domain patterns by using a separate control with a probe concentration of 0.4%. No discernible differences were found in this case. The lipid dyes RhPE and NaP prefer respectively the l_d and l_o phases, as checked by independent Laurdan GP experiments. Glucose, sucrose and $MgCl_2$ were from Sigma. Ultra-pure MilliQ water (18.3 M Ohm cm) was used in all steps involving water. A mica sheet (Plano GmbH, Wetzlar, Germany) of size 1 cm × 1 cm was glued on a round glass coverslip of diameter 24 mm using a biocompatible silicon glue (NuSil Technology, Carpinteria CA, USA). These substrate samples were used for membrane fixation and in AFM and epi-fluorescence imaging. The osmolarity of solutions was checked using an osmometer (Osmomat 030, Gonotec GmbH, Berlin, Germany).

2.1. Preparation of giant unilamellar vesicles (GUVs)

Electroformation is a widely known method for the preparation of GUVs [20]. We use a home-made electroformation chamber consisting of two parallel Pt-wires, connected to an external AC power-supply. We coat each of the two Pt-wires with 2 μl of the lipid solution (1 mM, in chloroform) using a Hamilton syringe. The chamber is then stored overnight in vacuum. To form vesicles by electroformation, the chamber is filled with 200 mM sucrose (400 μl) and an AC-voltage is applied at 55 °C in the following sequence: 10 Hz (0.2 VPP (peak-to-peak voltage) for 5 min, 0.5 VPP for 10 min, 1 VPP for 20 min, 1.5 VPP for 20 min, 2 VPP for 30 min), 4 Hz (2 VPP for 30 min). Finally, the temperature of the chamber is decreased to 23 °C at a rate of 0.02 °C/min before experiments at room temperature.

2.2. Epi-fluorescence microscopy

A Nikon TE2000 inverted microscope with 40X long working distance objective (Nikon ELWD, Plan Fluor, NA = 0.6) was used for epi-fluorescence observations. All experiments were done at room temperature (22 °C). Fluorescence excitation of the RhPE probe was done at 540 nm using a Xenon lamp (Polychrome V, Till Photonics GmbH, Grafeling, Germany) and a G-2A filter cube (Nikon) was used for imaging. Fluorescence images were recorded with an em-CCD camera (Sensicam em, 1004 × 1002 pixels, PCO-imaging, Kelheim, Germany) operated with TILLvision software (Till Photonics GmbH). Epi-fluorescence images were analyzed with Matlab (Mathworks, Natick MA, USA) and ImageJ (National Institute of Health, Bethesda MD, USA).

2.3. AFM imaging

Atomic force microscopy was performed using a JPK Nanowizard AFM (JPK Instruments, Berlin, Germany) operated in intermittent contact mode in fluid. The AFM was mounted on the epi-fluorescence microscope described above. Silicon cantilevers for soft-tapping were used (PPP-NCST-50, Nanosensors, Neuchatel, Switzerland), having a spring constant of 1.2–29 mN/m and a resonance frequency of 76–263 kHz. During scanning, the sample was located in a fluid cell (BioCell, JPK Instruments), with freshly cleaved mica on round coverslips as the substrate. The same cell was also used for epi-fluorescence imaging. AFM images were processed and analyzed using the programs SPIP (Image Metrology, Horsholm, Denmark) and Matlab.

2.4. Confocal microscopy

For confocal microscopy, vesicles were transferred to an eight-well microscopy chamber (Nunc Lab-Tek, Thermo Scientific, Waltham MA, USA) and observed by a Zeiss LSM 510 Meta confocal laser scanning fluorescence microscope (Carl Zeiss GmbH, Jena, Germany). Images were obtained with a 40X, C-Apochromat, water immersion objective with NA = 1.2. Two-channel image stacks were acquired using multi-track mode, using Argon lasers of wavelengths 458 nm and 543 nm, for NaP and RhPE excitation, respectively. The lasers were directed to the sample using two dichroic mirrors (HFT 458/514, HFT 488/543/633) for exciting NaP and RhPE respectively. Fluorescence emission was collected with photo-multiplier-tube (PMT) detectors. A beam splitter was used to eliminate remnant scattering from the laser sources (NFT 545) in a two-channel configuration. Additional filters were incorporated in front of the PMT detectors in the two different channels to measure the fluorescent intensity, i.e. a long-pass filter (>560 nm) for RhPE and a band-pass filter (500 ± 20 nm) for NaP. The acquired intensity images were checked to avoid PMT saturation and loss of offsets by adjusting the laser power, the detector gain and the detector offset. The image stacks were acquired above the Nyquist frequency. The raw confocal fluorescence image stacks were used for analysis without deconvolution. All confocal experiments were performed at room temperature.

3. Results

We examine ternary DOPC/DPPC/cholesterol membranes in the l_o, l_d coexistence region and characterize the domain patterns in free-standing GUVs and in planar patches resulting from collapse of the individual GUVs. We have opted for three different lipid compositions: Two inside the liquid–liquid coexistence region (*I* and *II*) while the third composition (*III*) is located close to the critical point [21], as shown schematically, in the phase diagram of Fig. 1A. The area-fraction of the two membrane phases is a sensitive indicator of the thermodynamic state of the membrane. For this reason we are quantifying the domain area-fraction to test for changes in the membrane state which could potentially be induced by fusion of the membrane to the solid support.

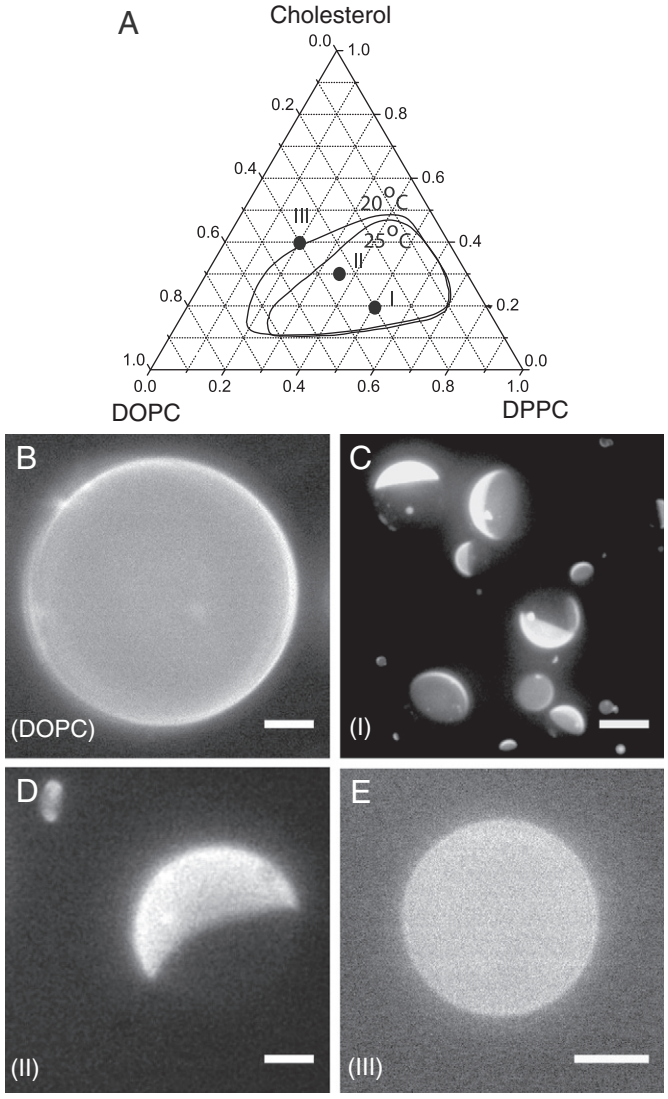

Fig. 1. Phase diagram (A) of the ternary system at two different temperatures (taken from [21]) and with the location of the three selected compositions (*I*, *II*, *III*) indicated. Epi-fluorescence micrographs of GUVs before rupture, prepared using (B) DOPC, (C) composition *I*, (D) composition *II* and (E) composition *III*. All membranes are labeled with RhPE. Bright and dark regions represent the l_d and l_o phases respectively. Scale bar is 10 μm.

3.1. Quantification of domain areas in GUVs

For confocal microscopy, the GUVs loaded with 200 mM sucrose solution were transferred to a microscopy chamber containing an osmotically matched glucose solution. Fig. 1B–E shows GUVs prepared using DOPC and the compositions *I*, *II* and *III*, respectively, settled at the bottom of the chamber, as observed in the epi-fluorescence mode. In Fig. 1C and D, round, micron sized, domain structures are visible. In contrast, the two lipid dyes are uniformly distributed in GUVs prepared using composition *III* and domains are not resolved, as shown in Fig. 1E. The area of domains in GUVs is quantified by applying the method developed by Husen et al. [22]. Here, a 3D-analysis of confocal image stacks of GUVs having lateral phase coexistence was developed. It was also found that GUVs formed from simple two- and three-component lipid mixtures by standard vesicle formation techniques, individually have a lipid composition corresponding to the global composition in the entire batch [22–24]. This gives us confidence in the application of compositionally complex GUVs for quantitative characterization of membrane phenomena.

The quantification of domain areas in phase separated GUV uses the fluorescence signal in the RhPE and NaP channels which originate from the l_d and l_o phases, respectively. For each point on a GUV, the RhPE and NaP intensities are measured and this allows the construction of a 2D-histogram indicating how much any combination of the two emission intensities contributes to the area of the GUV. Fig. 2A–C shows typical histograms of the RhPE versus NaP intensities in GUVs made with compositions *I*–*III*. For compositions *I* and *II*, it is clear that the two dyes preferentially segregate into two environments (l_d and l_o), as indicated by the formation of two separate regions in the histogram. For composition *III*, the analysis shows no such separation of the histogram, indicating a membrane without phase separation. When present, two well-separated regions in the histogram provide an unambiguous way to detect the domain areas since this can simply be found as the contribution to the area from each separate region in the histogram [22–24]. The determination of domain areas does not rely on the detection of individual domains, but is inferred from the distribution of pixel intensities. For compositions *I* and *II*, the l_o phase occupies 59.3 ± 3.3% (N = 7) and 55.7 ± 1.6% (N = 22) of the vesicle surface, respectively. The error bars (standard error of the mean = SEM) are similar to those found in our earlier analysis for various lipid compositions used to construct the ternary phase diagram [22]. The numbers for the area fractions are consistent with recent measurements of tie-lines in the same system [24].

3.2. Optimization of a protocol to capture fluid domains on mica

Fusion of single-phase GUVs to perforated supports in the presence of millimolar Ca^{2+} concentrations was previously reported by

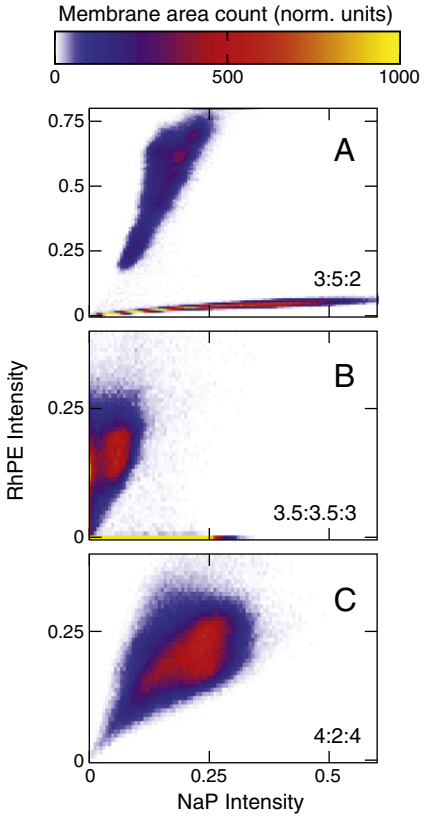

Fig. 2. Using confocal fluorescence images of GUVs to determine domain areas for the l_d and l_o phases. The 2D histograms in (A,B,C) show the contribution to the total GUV area (area count) from any combination of RhPE and NaP emission intensity. The histograms represent GUVs made from each of the compositions *I* (A), *II* (B) and *III* (C). In the case of phase separated GUVs (A,B) the RhPE will mainly partition into the l_d phase and NaP mainly into the l_o phase. The domain areas are determined as the area contributed from each of the two separate distributions in the histogram.

Heinemann et al. [25] and by Buchholz et al. [26]. The spreading of anionic multi-lamellar vesicles (MLVs) on glass, mediated by divalent cations, has been described by Orwar et al. [27] and other studies have reported the fusion of small unilamellar vesicles (SUVs) of zwitterionic DOPC on glass [28] or mica [29] as promoted by Ca^{2+} ions. We have explored the effect of divalent Mg^{2+} ions to optimize a procedure for capturing membrane domains on mica, starting from the free-standing GUVs. Below, the development of this procedure is outlined.

The required first step is to bring the GUVs in close contact with the mica surface. This is done by transferring the GUVs prepared in 200 mM sucrose solution into an AFM fluid chamber containing 1 ml of an isoosmolar glucose solution. Within a few minutes of transfer the GUVs settle on the mica, as shown in Fig. 3A. The domain structures present in free-floating GUVs are preserved after settling, with negligible shape perturbations [30]. When contact between GUVs and mica is established, the Mg^{2+} solution is introduced to promote rupture of the vesicles on mica. A titration strategy was initially employed where 2 mM Mg^{2+} solution, was titrated into the sample cell up to 500 μl (~1000 nmol Mg^{2+}). The osmolarity in the chamber was decreased by 50 mM and as a result the vesicles became tense, but remained intact. Another strategy consisted of adding low volumes of more concentrated Mg^{2+} to maintain a relatively constant osmotic pressure difference across the membrane. Within ~2 days after adding 2 μl of 100 mM Mg^{2+} solution (~200 nmol Mg^{2+}) the GUVs do not adhere to the mica surface. Interestingly, if a Mg^{2+} solution of a slightly higher concentration is introduced at the center of the chamber, but not the edge, the adsorption followed by rupture of GUVs occurs. The mechanism thus appears to be that the salt solution, when added at the center, will efficiently sink to the vesicles settled on the mica. When compared to the titration strategy it is clear that the important step for promoting membrane adhesion and rupture is to locally deliver a sufficiently high Mg^{2+} concentration to the GUV/mica interface. This conforms with micropipette experiments by Orwar et al. which showed membrane binding induced by locally delivered divalent cations [27]. We note that since the Mg^{2+} solution is introduced from the top while the GUV adheres to the substrate from below, the GUV will be immersed in Mg^{2+} ions during spreading and rupture. Taken together with the fast diffusion of Mg^{2+} ions in water ($D \sim 0.7 \cdot 10^{-5}$ cm^2/s [31]), the transport of divalent ions will not be limiting the fusion of GUVs.

To summarize, a minimal concentration has been identified, where planar membrane patches are formed from GUVs, while retaining their area and round fluid domain shapes. In all experiments described here, we have added 1 μl of a 274 mM $MgCl_2$ stock solution, at the center of the chamber. For reference we note that the typical physiological concentration of Ca^{2+}-ions is on the order of 1 mM [32,33].

Upon addition of the Mg^{2+} ions to the chamber, the vesicles which were already settled on the mica immediately ruptured to form planar membrane patches, as shown in Fig. 3B. Vesicles, which were not settled on the mica, remained unaffected after adding Mg^{2+} ions. The dynamics of the rupture process is illustrated in Supplementary material 1 (Movie1.avi).

3.2.1. Rupture mechanism and time-scale of rupture

During formation of a patch, the outer leaflet of the vesicle adsorbs to the mica while the inner leaflet becomes exposed to the bulk solution after rupture of the vesicle. As a confirmation of this, we found that the outermost membrane of a multi-lamellar vesicle opens up to eject the solvent and an internal vesicle, as shown in Fig. 4A–C. The internal vesicle is now diffusing freely on top of the membrane patch formed by the external vesicle implying that it is not adhered to the patch. The internal vesicle ruptures only when it diffuses out of the patch and comes into direct contact with mica, as shown in Fig. 4D.

The mechanism for formation of a planar membrane patch can be summarized as follows: In the presence of Mg^{2+} ions, the outer membrane of a GUV, which is in contact with the support, becomes adhered, thus making the vesicle tense due to the fixed enclosed volume. As a result, an increasing amount of fluctuating pores starts to form in the membrane and eventually a single pore surpasses the critical size leading to rupture of the GUV. The dynamics of tension-induced rupture of membranes is well established by e.g. E. Evans and coworkers [34,35]. This work employs a single-hole model which accurately reproduces the experimental data. The time-scale for opening a hole as induced by micropipette aspiration was experimentally found to have an upper limit of 10 ms and theoretically estimated to be 30–100 μs [34]. The time scale for hole opening is fundamentally set by the tension loading-rate and intrinsic membrane properties such as the edge energy of holes. Likewise, single pore-opening and rupture of GUVs on a glass-support were resolved by high-speed imaging by Hamai et al. reporting a time scale for hole-opening of 10 ms [36]. These authors also reported a close correlation between the patch shape and the position of the expanding hole. We observe both circular and non-circular shaped patches in our experiments, in agreement with this study. The frame-rate in our experiments does not resolve the actual rupture process, but based on the previously established features of hole-opening we assume a time-scale of ~10 ms.

From the arguments given above, we find that the rupture event followed by adsorption of GUVs, is so rapid that no lateral rearrangement of the fluid domain patterns is possible. To support this claim, a simple check can be made to examine the hypothetical possibility that membrane domains are reorganized during the fusion process from interactions with the solid support. With a lipid diffusion coefficient in the fluid phase of $D \sim 10^{-12}$ m^2/s and a speed of the adhesion-front (for a 10 μm vesicle say) of the order of $\dot{R} \sim 10^{-3}$ m/s, the minimum domain size which can be captured on the support becomes, $D/\dot{R} \sim 1$ nm. This number effectively provides an order-of-magnitude estimate of the resolution of the domain size in the free standing membranes.

3.3. High-resolution imaging of membrane patches by AFM

The planar membrane patches have been investigated thoroughly with AFM. For reference, Fig. 5A shows an epi-fluorescence image of a membrane patch formed by rupture of vesicles prepared with composition *I*. The round shaped l_o, l_d lateral domains present in GUVs have

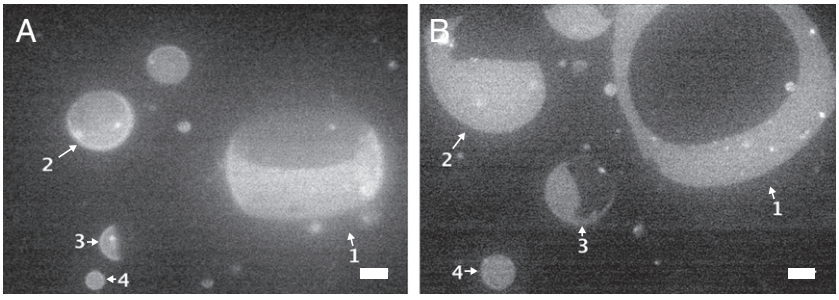

Fig. 3. Illustration of the pre- and post-rupture state of GUVs. Epi-fluorescence image (A) of GUVs settled on mica without Mg^{2+} ions, (B) planar bilayer patches formed upon addition of Mg^{2+} ions. The numbers and arrows show matching pairs of vesicles and patches in (A) and (B) respectively. GUVs were prepared using the composition *I*. Scale bar is 10 μm.

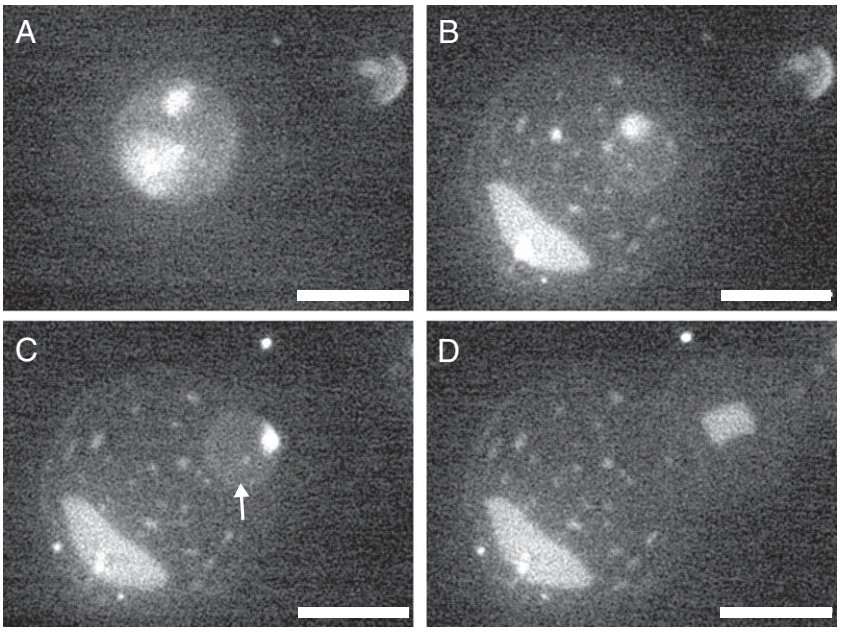

Fig. 4. Two-stage rupture of a multilamellar GUV with composition *I*. Fluorescence image (A) of a multilamellar GUV settled on mica without Mg^{2+} ions. The outermost GUV has adsorbed and ruptured on mica after addition of Mg^{2+} (B) releasing an intact inner vesicle and forming a planar patch. The inner vesicle (C) diffuses on top of the bilayer patch (arrow). Rupture of the inner vesicle (D) happens when it has traveled to a region with freely exposed mica substrate. Scale bar is 10 μm.

retained their shape, after the vesicles have ruptured on mica. The figure shows patches from two vesicles that are joined at their edges. This pattern may result from the fusion of an external vesicle followed by an internal vesicle, as discussed above in Fig. 3, or could be from two originally separate vesicles. Fig. 5B shows an AFM scan of the same vesicle patch on mica. Fig. 5C shows the area distribution of the two liquid phases, where green and red colors represent the l_o, l_d phases respectively. Fig. 5D shows the AFM height line scan for the profiles indicated in Fig. 5B, revealing that the patch is one bilayer thick, with a thickness of 3.25 ± 0.25 nm in the l_d phase. A height difference of 1.0 ± 0.2 nm is observed between thick and thin regions within the membrane patch. This agrees well with the height difference between the l_o (thick) and l_d (thin) regions, as previously reported [10].

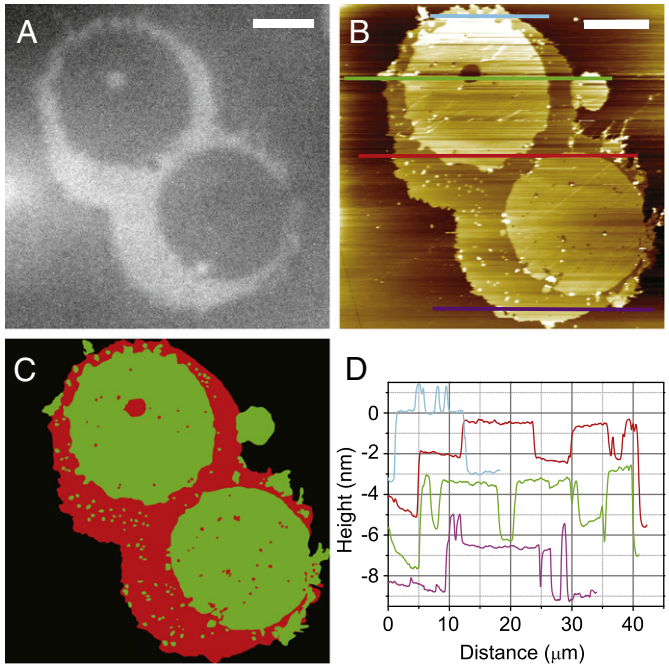

Fig. 5. Co-localized AFM and fluorescence imaging of patches formed from ruptured GUVs with composition *I*. Epi-fluorescence image (A) of a patch made from two adjoining ruptured GUVs. AFM topography image (B) of the same patch region. Binary segmentation (C) of the AFM image into coexisting phases with green and red representing the l_o and l_d phases respectively. Height profiles (D) of the color-coded lines as indicated in (B). Scale bar is 10 μm.

Fig. 6A shows a vesicle patch with composition *II* corresponding to a composition closer to the critical point than composition *I*. Nano- and micro-scale domain structures belonging to the thinner phase are abundant in the top part of the patch in Fig. 6B. AFM height profiles confirm that these are l_d phase domains embedded in a surrounding l_o phase. The lower part of the patch contains an equivalent, but inverted pattern with small-scale domains of the l_d phase surrounded by the l_o phase.

Fig. 6C shows a segmentation of the AFM image where the green and red colors represent the l_o and l_d phases respectively. The height difference between the domains as given in Fig. 6D is around 0.6 ± 0.05 nm. This is lower than that of composition *I* agreeing well with the fact that composition has moved from deep in l_o,l_d co-existence region in the ternary phase diagram towards a critical point, where both the l_o ,l_d phases have similar thickness. The average bilayer thickness is found to be 3.25 ± 0.25 nm in the l_d phase.

Fig. 7A shows a vesicle patch of composition *III*. This lipid composition is near the critical point in the ternary phase diagram [21]. The AFM topography image in Fig. 7B does not reveal extended areas on the bilayer patch corresponding to domain formation. This may be attributed to a system being in a super-critical state (one phase) or being in a near-critical state (two phases) where phases are indistinguishable by AFM and fluorescence. This bilayer thickness is found to be around 3.25 ± 0.25 nm.

Small l_o domains within the l_d phase and vice-versa, are consistently observed in AFM images of patches with compositions *I* and *II*. These domain features have sizes ranging from the nanometer to the micrometer scale and thus are more close to the presumed size of functional biomembrane domains in cellular systems. It is therefore of interest to examine these features more closely.

Fig. 8A and B shows epi-fluorescence images of two bilayer patches, prepared using the composition *I*, and Fig. 8C and D shows corresponding AFM images obtained at high pixel resolution. Small-scale domains of elevated and depressed regions are abundant in the AFM images but these are not resolvable in the epi-fluorescence images of the

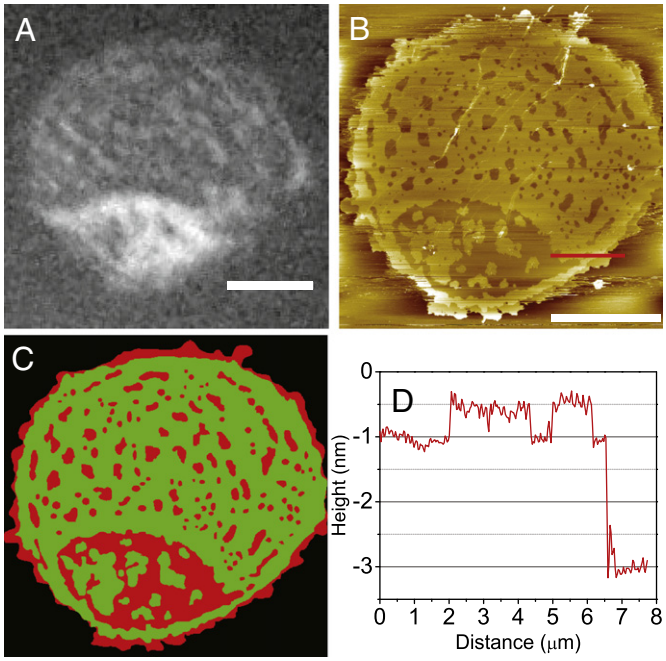

Fig. 6. Co-localized AFM and fluorescence imaging of patches formed from ruptured GUVs with composition *II*. Epi-fluorescence image (A) of a planar patch and the corresponding topographical AFM image (B) of the same patch. Binary segmentation (C) of the AFM image into coexisting phases with green and red representing the l_o and l_d phases respectively. Topography profile (D) of the line (red) indicated in (B). Scale bar is 10 μm.

same patch. A step height difference of 0.9 ± 0.1 nm confirms the l_o,l_d phase character of these domains. Besides the macroscopic round domain structures observable with fluorescence microscopy we find that both the l_o and l_d phases are decorated with small-scale domains of the opposite phase. For the l_d phase these domains are prevalent even deep in the l_o,l_d coexistence region.

The general interpretation of our observations with compositions *I* and *II* is that the membrane patches, when viewed at optical resolution, appear to display complete phase separation with two sharply defined regions belonging to each fluid phase. However, when viewed in high-resolution AFM, small domains below the optical resolution limit are prominent within both of the two major phase regions.

Most of the observed patches have edges ending in the l_d phase. This gives us an indication that a pore leading to the rupture event must have formed in this phase. It confirms well with the fact that formation of a pore in the l_d phase is energetically favorable due to a lower edge energy, as compared to that in the l_o phase [37,38].

Another distinct observation is the presence of elongated domains aligned perpendicular to the boundary of the patch, as present in Figs. 6 and 8. The apparent elongation and orientation of domains are a result of the fusion process. The spreading of a quasi-spherical GUV

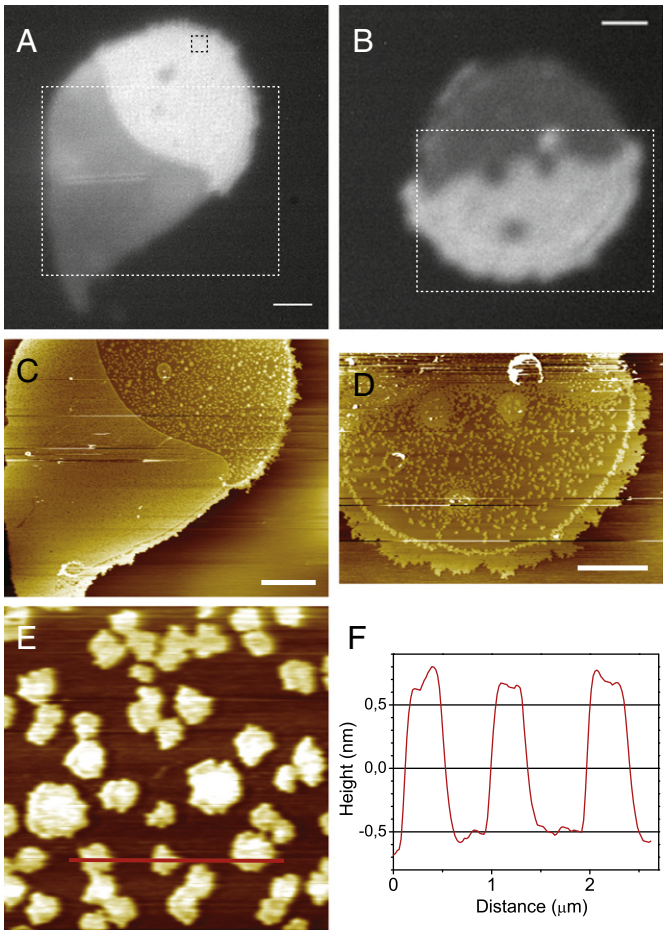

Fig. 8. Small-scale domain patterns coexisting with macroscopic l_d,l_o phase separation in two patches with composition *I*. Epi-fluorescence images (A,B) and matching AFM topography images (C,D,E). The regions of the AFM images are indicated with squares in panel labels A and B. The topography profile in (F) corresponds to the line (red) in (E). Scale bar is 10 μm.

on a solid support is associated with lateral shearing such that domains appear stretched in the direction perpendicular to the spreading direction. The region most strongly influenced by such deformations will be the region closest to the expanding hole which becomes the perimeter of the patch where the expanding hole was located.

We finally determine the area-fraction of the l_o and l_d phases in the AFM images. We calculated the number of pixels covered by the l_o and l_d phases to calculate the respective area-fraction. Figs. 5D and 6D show the result of the quantification of the AFM image analysis, where green color represents the l_o phase and red color represents the l_d phase. The results found by the analysis of patches revealed that the

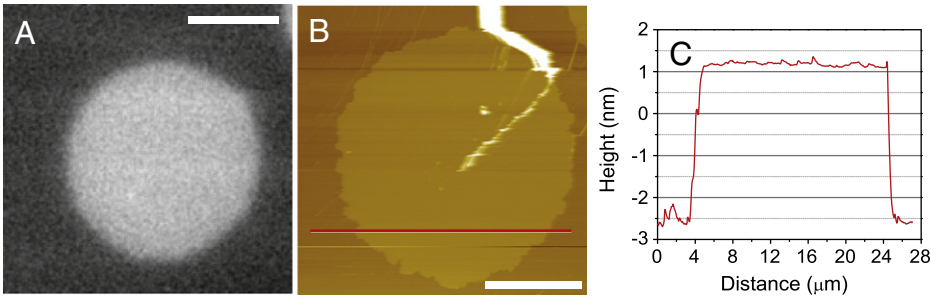

Fig. 7. Fluorescence (A) and AFM (B) image of a membrane patch with composition *III*. Domains are not resolved for this composition. Topography profile (C) for the line (red) indicated in (B). Scale bar is 10 μm.

vesicles prepared with composition *I* have 58.2 ± 2.5% (N = 10) of the total patch area in the l_o phase. For composition *II* the result is that the l_o phase constitutes 56.8 ± 3.7% (N = 8) of the total patch area. We did not observe any membrane reorganization in the patches over a time-scale of hours.

4. Discussion and conclusions

The stability of multi-component lateral structures of lipid membranes is often marginal and easy to modify by low-energy perturbations from the environment like a solid support. Therefore, the stabilization techniques required for high-resolution imaging of membranes are prone to exert an influence on the lateral structure and must be used with care. We have presented a methodology which allows imaging of the lateral structure and lipid micro-domains of free-standing vesicles by rapid transferal of individual GUVs to a solid support, where the membrane-support interactions are exploited differently than in conventional supported membrane studies. The method can be considered as a supplement to spectroscopic techniques like NMR, ESR [6] and fluorescence spectroscopy [39,40], as well as single-particle tracking experiments [41]. All these techniques only indirectly provide structural information on free-standing membranes in a model-dependent manner.

To validate our procedure, the well-investigated ternary model membrane system consisting of DOPC, DPPC and cholesterol was chosen. While macroscopic domains associated with phase separation in free-standing membranes are well described for this system, small-scale domains have not been imaged. GUVs were prepared with two compositions in the l_o,l_d coexistence region at room temperature and one composition close to the l_o,l_d critical point.

The compositional dispersity among vesicles for a given overall lipid composition was minimal as checked by measuring the area fractions of l_o and l_d phases in each vesicle, using confocal fluorescence microscopy. After transferal to the solid support, the area fractions of l_o and l_d regions were again analyzed based on AFM images, revealing that it remained unchanged with no lateral reorganization of the membrane being resolved over a time-scale of hours. This fact supports our hypothesis that the adsorption event is fast compared to the in-plane diffusion of membrane lipids and that there is no time for lateral re-distribution of lipids on length scales above ~1 nm. The fact that we measure similar area fractions in GUVs and patches indicates that the lipid composition among vesicles remains stable throughout the different preparation steps.

The agreement between domain area fractions for domains in GUVs and patches together with the short time-scale for collapse suggests that the membrane patch retains information about the domain pattern in the original free-standing GUV. The sensitivity of the area fraction to the thermodynamic state of the membrane serves as general control that this state is not measurably shifted during patch formation. Specifically, this speaks against small domains being induced by interactions between the membrane and the solid support. The presence of deformed domains created during rupture of the GUV also supports that the domain pattern in the free-standing membrane is maintained in the patch.

Another mechanism by which the domain pattern could be speculated to change during rupture is via lateral tension. A change in membrane tension can and will shift the equilibrium between the l_o and l_d phases [42]. However, lateral equilibration is slow compared to the fusion time for the GUV and our check of the area fraction confirms that this equilibration has not taken place prior to fixation. Moreover, tension will drive the system towards a lower proportion of the l_o phase which cannot explain our observations of small-scale l_o domains. Finally, the central part of patches will have adhered to the substrate first and at low tension, but these regions also exhibit small-scale domains (see e.g. Fig. 8D) which can therefore not have been induced by tension.

The patches were analyzed by the high-resolution microscopy technique AFM to reveal patterns of small domains. We found that the height difference between domains of all sizes is consistent with previous AFM measurements of l_o,l_d coexistence using conventional supported membranes. Small-size l_o domains proliferated in the l_d phase and vice-versa were consistently observed for compositions *I* and *II* in the co-existence region. The characteristic domain-size increases as the composition approaches the critical point.

Since some lipid diffusion may be present in the patches, the small-size domains could hypothetically have been nucleated after fusion to the support. A strong argument against this hypothesis is that small domains of both the l_o and l_d phases coexist for compositions *I* and *II*. The existence of small domains of both phases is difficult to reconcile with a thermodynamically driven nucleation process. If the small domains were indeed a result of a change in phase state, we would expect one of the phases to increase and the other phase to decrease. In fact, thermodynamic nucleation cannot produce small domains of the l_d phase. An increase in the ld phase is equivalent to melting which will happen along the existing l_o–l_d phase boundary.

The small-scale domains can instead be considered as a manifestation of pseudo-critical fluctuations which are present in the ternary lipid mixture over a wide range of compositions displaying l_o,l_d coexistence. The interpretation of the small domains being fluctuations is in agreement with measurements of domain line tension λ obtained by epi-fluorescence of GUVs of the same mixtures, where λ ~ 0.1 pN over a wide range of temperatures [43], suggesting spontaneous formation of nano-domains up to $\frac{k_B T}{\lambda}$~100 nm size. Time sequences of GUVs reported by Veatch et al. indicate fluctuating domains below the critical point, where two distinct phases are observable with fluorescence microscopy. However, for the compositions in the deep coexistence region these fluctuations decrease in size and are not resolved optically [16]. A similar behavior is found in one-component saturated and mono-unsaturated lipid bilayers near the main transition, where pseudo-critical fluctuations resulting in micro-domains are found, despite the fact that the nearness of a critical point is varying considerably [17,44–46]. The fluctuation phenomena described above, even for a single-component system, have major implications for membrane properties, such as mechanics [47] and permeability [48]. Furthermore, they provide a mechanism for lipid aggregation and stabilization of lipid–protein complexes, away from coexistence [49]. The presented technique opens the possibility to image such phenomena in free-standing membranes at length and time scales that previously were not accessible.

Supplementary data to this article can be found online at http://dx.doi.org/10.1016/j.bbamem.2014.05.016.

Acknowledgements

We thank the Danish Council for Independent Research | Natural Sciences (FNU), grant number 95-305-23443 for the financial support. Experiments where carried out on the facilities of DaMBIC - Danish Molecular Biomedical Imaging Center.

References

[1] K. Simons, E. Ikonen, Functional rafts in cell membranes, Nature 387 (6633) (1997) 569–572, http://dx.doi.org/10.1038/42408.
[2] J. Ipsen, G. Karlstrom, O. Mouritsen, H. Wennerstrom, M. Zuckermann, Phase-equilibria in the phosphatidylcholine–cholesterol system, Biochim. Biophys. Acta 905 (1) (1987) 162–172, http://dx.doi.org/10.1016/0005-2736(87)90020-4.
[3] C. Dietrich, L. Bagatolli, Z. Volovyk, N. Thompson, M. Levi, K. Jacobson, E. Gratton, Lipid rafts reconstituted in model membranes, Biophys. J. 80 (3) (2001) 1417–1428, http://dx.doi.org/10.1016/S0006-3495(01)76114-0.
[4] R. Parton, M. Hanzal-Bayer, J. Hancock, Biogenesis of caveolae: a structural model for caveolin-induced domain formation, J. Cell Sci. 119 (5) (2006) 787–796, http://dx.doi.org/10.1242/jcs.02853.
[5] K. Simons, M.J. Gerl, Revitalizing membrane rafts: new tools and insights, Nat. Rev. Mol. Cell Biol. 11 (10) (2010) 688–699, http://dx.doi.org/10.1038/nrm2977.

[6] M. Vist, J. Davis, Phase-equilibria of cholesterol dipalmitoylphosphatidylcholine mixtures — H2 nuclear magnetic resonance and differential scanning calorimetry, Biochemistry 29 (2) (1990) 451–464, http://dx.doi.org/10.1021/bi00454a021.
[7] C. Eggeling, C. Ringemann, R. Medda, G. Schwarzmann, K. Sandhoff, S. Polyakova, V. N. Belov, B. Hein, C. von Middendorff, A. Schoenle, S.W. Hell, Direct observation of the nanoscale dynamics of membrane lipids in a living cell, Nature 457 (7233) (2009) 1159–1162, http://dx.doi.org/10.1038/nature07596.
[8] C. Scomparin, S. Lecuyer, M. Ferreira, T. Charitat, B. Tinland, Diffusion in supported lipid bilayers: influence of substrate and preparation technique on the internal dynamics, Eur. Phys. J. E 28 (2) (2009) 211–220, http://dx.doi.org/10.1140/epje/i2008-10407-3.
[9] D. Keller, N. Larsen, I. Moller, O. Mouritsen, Decoupled phase transitions and grain-boundary melting in supported phospholipid bilayers, Phys. Rev. Lett 94 (2) (2005), http://dx.doi.org/10.1103/PhysRevLett.94.025701.
[10] M.H. Jensen, E.J. Morris, A.C. Simonsen, Domain shapes, coarsening, and random patterns in ternary membranes, Langmuir 23 (15) (2007) 8135–8141, http://dx.doi.org/10.1021/la700647v.
[11] J.C. Stachowiak, F.M. Brodsky, E.A. Miller, A cost–benefit analysis of the physical mechanisms of membrane curvature, Nat. Cell Biol. 15 (9) (2013) 1019–1027, http://dx.doi.org/10.1038/ncb2832.
[12] T. Gil, J. Ipsen, O. Mouritsen, M. Sabra, M. Sperotto, M. Zuckermann, Theoretical analysis of protein organization in lipid membranes, Biochim. Biophys. Acta Rev. Biomembr. 1376 (3) (1998) 245–266, http://dx.doi.org/10.1016/S0304-4157(98)00022-7.
[13] F. Tokumasu, A. Jin, G. Feigenson, J. Dvorak, Nanoscopic lipid domain dynamics revealed by atomic force microscopy, Biophys. J. 84 (4) (2003) 2609–2618, http://dx.doi.org/10.1016/S0006-3495(03)75066-8.
[14] L. Tamm, H. McConnell, Supported phospholipid-bilayers, Biophys. J. 47 (1) (1985) 105–113, http://dx.doi.org/10.1016/S0006-3495(85)83882-0.
[15] P. Milhiet, M. Giocondi, C. Grimellec, AFM imaging of lipid domains in model membranes, Sci. World J. 17 (2003) 59, http://dx.doi.org/10.1100/tsw.2003.12.
[16] A.R. Honerkamp-Smith, B.B. Machta, S.L. Keller, Experimental observations of dynamic critical phenomena in a lipid membrane, Phys. Rev. Lett 108 (26) (2012), http://dx.doi.org/10.1103/PhysRevLett.108.265702.
[17] J. Ipsen, K. Jorgensen, O. Mouritsen, Density fluctuations in saturated phospholipid-bilayers increase as the acyl-chain length decreases, Biophys. J. 58 (5) (1990) 1099–1107, http://dx.doi.org/10.1016/S0006-3495(90)82452-8.
[18] W. Knoll, G. Schmidt, E. Sackmann, K. Ibel, Critical demixing in fluid bilayers of phospholipid mixtures — a neutron-diffraction study, J. Chem. Phys. 79 (7) (1983) 3439–3442, http://dx.doi.org/10.1063/1.446193.
[19] W. Knoll, K. Ibel, E. Sackmann, Small-angle neutron-scattering study of lipid phase — diagrams by the contrast variation method, Biochemistry 20 (22) (1981) 6379–6383, http://dx.doi.org/10.1021/bi00525a015.
[20] M. Angelova, S. Soleau, P. Meleard, J. Faucon, P. Bothorel, Preparation of giant vesicles by external AC electric-fields — kinetics and applications, in: C. Helm, M. Losche, H. Mohwald (Eds.), Trends in Colloid and Interface Science VI, Prog. Coll. interf. Sci., vol. 89, 1992, pp. 127–131, http://dx.doi.org/10.1007/BFb0116295.
[21] S. Veatch, S. Keller, Separation of liquid phases in giant vesicles of ternary mixtures of phospholipids and cholesterol, Biophys. J. 85 (5) (2003) 3074–3083, http://dx.doi.org/10.1016/S0006-3495(03)74726-2.
[22] P. Husen, M. Fidorra, S. Haertel, L.A. Bagatolli, J.H. Ipsen, A method for analysis of lipid vesicle domain structure from confocal image data, Eur. Biophys. J. Biophys. Lett. 41 (2) (2012) 161–175, http://dx.doi.org/10.1007/s00249-011-0768-2.
[23] M. Fidorra, A. Garcia, J.H. Ipsen, S. Haertel, L.A. Bagatolli, Lipid domains in giant unilamellar vesicles and their correspondence with equilibrium thermodynamic phases: a quantitative fluorescence microscopy imaging approach, Biochim. Biophys. Acta Biomembr. 1788 (10) (2009) 2142–2149, http://dx.doi.org/10.1016/j.bbamem.2009.08.006.
[24] P. Husen, L.R. Arriaga, F. Monroy, J.H. Ipsen, L.A. Bagatolli, Morphometric image analysis of giant vesicles: a new tool for quantitative thermodynamics studies of phase separation in lipid membranes, Biophys. J. 103 (11) (2012) 2304–2310, http://dx.doi.org/10.1016/j.bpj.2012.10.031.
[25] F. Heinemann, P. Schwille, Preparation of micrometer-sized free-standing membranes, ChemPhysChem 12 (14) (2011) 2568–2571, http://dx.doi.org/10.1002/cphc.201100438.
[26] K. Buchholz, A. Tinazli, A. Kleefen, D. Dorfner, D. Pedone, U. Rant, R. Tampé, G. Abstreiter, M. Tornow, Silicon-on-insulator based nanopore cavity arrays for lipid membrane investigation, Nanotechnology 19 (44) (2008) 445305, http://dx.doi.org/10.1088/0957-4484/19/44/445305.
[27] T. Lobovkina, I. Gozen, Y. Erkan, J. Olofsson, S.G. Weber, O. Orwar, Protrusive growth and periodic contractile motion in surface-adhered vesicles induced by Ca^{2+}-gradients, Soft Matter 6 (2) (2010) 268–272, http://dx.doi.org/10.1039/b916805m.
[28] R. Richter, A. Mukhopadhyay, A. Brisson, Pathways of lipid vesicle deposition on solid surfaces: a combined QCM-D and AFM study, Biophys. J. 85 (5) (2003) 3035–3047, http://dx.doi.org/10.1016/S0006-3495(03)74722-5.
[29] M. Benes, D. Billy, A. Benda, H. Speijer, M. Hof, W. Hermens, Surface-dependent transitions during self-assembly of phospholipid membranes on mica, silica, and glass, Langmuir 20 (23) (2004) 10129–10137, http://dx.doi.org/10.1021/la048811u.
[30] J. Henriksen, A. Rowat, J. Ipsen, Vesicle fluctuation analysis of the effects of sterols on membrane bending rigidity, Eur. Biophys. J. Biophys. Lett. 33 (8) (2004) 732–741, http://dx.doi.org/10.1007/s00249-004-0420-5.
[31] E. Cussler, Diffusion: Mass Transfer in Fluid Systems, Cambridge Series in Chemical Engineering, Cambridge University Press, 1997., http://dx.doi.org/10.2277/0521564778.
[32] W. Robertson, R. Marshall, G.N. Bowers, Ionized calcium in body fluids, Crit. Rev. Clin. Lab. Sci. 15 (2) (1981) 85–125, http://dx.doi.org/10.3109/10408368109105869.
[33] L. Larsson, S. Ohman, Serum ionized calcium and corrected total calcium in borderline hyperparathyroidism, Clin. Chem. 24 (11) (1978) 1962–1965.
[34] E. Evans, V. Heinrich, F. Ludwig, W. Rawicz, Dynamic tension spectroscopy and strength of biomembranes, Biophys. J. 85 (4) (2003) 2342–2350, http://dx.doi.org/10.1016/S0006-3495(03)74658-X.
[35] E. Evans, B.A. Smith, Kinetics of hole nucleation in biomembrane rupture, New J. Phys. 13 (9) (2011) 095010, http://dx.doi.org/10.1088/1367-2630/13/9/095010.
[36] C. Hamai, P.S. Cremer, S.M. Musser, Single giant vesicle rupture events reveal multiple mechanisms of glass-supported bilayer formation, Biophys. J. 92 (6) (2007) 1988–1999, http://dx.doi.org/10.1529/biophysj.106.093831.
[37] D. Needham, T. Mcintosh, E. Evans, Thermomechanical and transition properties of dimyristoylphosphatidylcholine/cholesterol bilayers, Biochemistry 27 (13) (1988) 4668–4673, http://dx.doi.org/10.1021/bi00413a013.
[38] T. Portet, R. Dimova, A new method for measuring edge tensions and stability of lipid bilayers: effect of membrane composition, Biophys. J. 99 (10) (2010) 3264–3273, http://dx.doi.org/10.1016/j.bpj.2010.09.032.
[39] P. Almeida, W. Vaz, T. Thompson, Lateral diffusion in the liquid-phases of dimyristoylphosphatidylcholine/cholesterol lipid bilayers — a free-volume analysis, Biochemistry 31 (29) (1992) 6739–6747, http://dx.doi.org/10.1021/bi00144a013.
[40] K. Gowrishankar, S. Ghosh, S. Saha, C. Rumamol, S. Mayor, M. Rao, Active remodeling of cortical actin regulates spatiotemporal organization of cell surface molecules, Cell 149 (6) (2012) 1353–1367, http://dx.doi.org/10.1016/j.cell.2012.05.008.
[41] C. Dietrich, B. Yang, T. Fujiwara, A. Kusumi, K. Jacobson, Relationship of lipid rafts to transient confinement zones detected by single particle tracking, Biophys. J. 82 (1) (2002) 274–284, http://dx.doi.org/10.1016/S0006-3495(02)75393-9.
[42] T. Portet, S.E. Gordon, S.L. Keller, Increasing membrane tension decreases miscibility temperatures; an experimental demonstration via micropipette aspiration, Biophys. J. 103 (8) (2012) L35–L37, http://dx.doi.org/10.1016/j.bpj.2012.08.061.
[43] A.R. Honerkamp-Smith, P. Cicuta, M.D. Collins, S.L. Veatch, M. den Nijs, M. Schick, S.L. Keller, Line tensions, correlation lengths, and critical exponents in lipid membranes near critical points, Biophys. J. 95 (1) (2008) 236–246, http://dx.doi.org/10.1529/biophysj.107.128421.
[44] M. Morrow, D. Singh, D. Lu, C. Grant, Glycosphingolipid fatty-acid arrangement in phospholipid-bilayers — cholesterol effects, Biophys. J. 68 (1) (1995) 179–186, http://dx.doi.org/10.1016/S0006-3495(95)80173-6.
[45] M.C. Rheinstaedter, J. Das, E.J. Flenner, B. Bruening, T. Seydel, I. Kosztin, Motional coherence in fluid phospholipid membranes, Phys. Rev. Lett 101 (24) (2008), http://dx.doi.org/10.1103/PhysRevLett.101.248106.
[46] C.L. Armstrong, D. Marquardt, H. Dies, N. Kucerka, Z. Yamani, T.A. Harroun, J. Katsaras, A.-C. Shi, M.C. Rheinstaedter, The observation of highly ordered domains in membranes with cholesterol, Plos One 8 (6) (2013), http://dx.doi.org/10.1371/journal.pone.0066162.
[47] T. Honger, K. Mortensen, J. Ipsen, J. Lemmich, R. Bauer, O. Mouritsen, Anomalous swelling of multilamellar lipid bilayers in the transition region by renormalization of curvature elasticity, Phys. Rev. Lett. 72 (24) (1994) 3911–3914, http://dx.doi.org/10.1103/PhysRevLett.72.3911.
[48] L. Cruzeiro-Hansson, J. Ipsen, O. Mouritsen, Intrinsic molecules in lipid-membranes change the lipid-domain interfacial area — cholesterol at domain interfaces, Biochim. Biophys. Acta 979 (2) (1989) 166–176, http://dx.doi.org/10.1016/0005-2736(89)90432-X.
[49] T. Gil, M. Sabra, J. Ipsen, O. Mouritsen, Wetting and capillary condensation as means of protein organization in membranes, Biophys. J. 73 (4) (1997) 1728–1741, http://dx.doi.org/10.1016/S0006-3495(97)78204-3.